

## DSM Generation and Interior Orientation Determination of IKONOS Images Using a Testfield in Switzerland\*

EMMANUEL BALTSAVIAS, ZHANG LI & HENRI EISENBEISS, Zürich

**Keywords:** photogrammetry, high-resolution satellite images, IKONOS, image matching, DSM generation, in-flight calibration, interior orientation

**Abstract:** We present processing of Ikonos triplet images over a testfield in Thun, Switzerland with accurate ground control points, 1600 m height range, variable land cover and suboptimal imaging conditions (snow, long shadows). A sophisticated matching algorithm for DSM generation is presented and the results are compared to reference data from airborne laser scanning. The RMS errors for the whole area, excluding vegetation, were 2–3 m, while for bare ground the accuracy is about 1 m or less. The accurate matching allowed the detection and quantification of errors in the interior orientation of the sensor, caused by changes in the relative position of the 3 CCDs forming the virtual CCD line. These errors were verified through a co-operation with Space Imaging and recomputation of the sensor interior orientation. The interior orientation errors caused height jumps of 1.3 to 1.5 m along two stripes at the overlap regions of the 3 CCDs. The method used for the detection and quantification of these errors is applicable for in-flight calibration of sensors forming a virtual image through butting of multiple CCD arrays, without the need of testfields with signalled points, which are difficult to establish and maintain. Depending on the accuracy of the matching method and of the reference DSM, we estimate that this in-flight calibration method can detect interior orientation errors causing parallax errors of 0.3–0.5 pixels or more.

**Zusammenfassung:** Erstellung eines digitalen Oberflächenmodells inkl. der Bestimmung der inneren Orientierung aus Ikonos Bildern eines Testgebietes in der Schweiz. In diesem Beitrag werden Ergebnisse eines Tests mit Ikonos-Triplet-Bildern präsentiert, die über Thun in der Schweiz aufgenommen wurden. Das Gebiet zeigt unterschiedliche Bodenbedeckung und Höhenunterschiede von ca. 1600 m. Genaue Pass- und Kontrollpunkte waren vorhanden, die Aufnahmebedingungen waren sub-optimal (Schnee, lange Schatten). Ein ausgefeilter Algorithmus zur Ableitung digitaler Oberflächenmodelle wird präsentiert, die Ergebnisse werden mit einem Referenzdatensatz, der über Laserscanning gewonnen wurde, verglichen. Der RMS Fehler beträgt für das gesamte Gebiet, unter Ausschluss der Vegetationsflächen, 2–3 m, während er im offenen Gelände 1 m oder besser ist. Die genaue Bildzuordnung und Quantifizierung von Fehlern der inneren Orientierung des Sensors, die durch Änderungen der relativen Lage der drei CCD Sensoren, die die virtuelle CCD Zeile bilden, hervorgerufen werden. Diese Fehler wurden im Rahmen einer Kooperation mit Space Imaging durch eine Neuberechnung der inneren Orientierung verifiziert. Die Fehler führten zu Höhensprüngen vom 1.3 m bzw. 1.5 m entlang zweier Streifen im Überlappungsbereich zwischen den drei CCD Sensoren. Die entwickelte Methode zur Erkennung und Quantifizierung dieser Fehler kann zur In-flight Kalibrierung von Sensoren verwendet werden, bei denen virtuelle Bilder durch Butting einzelner CCD Sensoren entstehen. Ein Testfeld mit signalisierten Punkten, das nur schwierig zu erstellen und zu pflegen ist, ist dafür nicht notwendig. Abhängig von der Genauigkeit der Bildzuordnung und der Referenzoberfläche wird geschätzt, dass Fehler der inneren Orientierung bestimmt werden können, die bzgl. der Parallaxe mindestens 0.3–0.5 Pixel betragen.

\* Enhanced version of a paper published in the proceedings of the ISPRS Hannover Workshop 2005 „High Resolution Earth Imaging for Geospatial Information“, May 17–20, 2005, Institute of Photogrammetry and GeoInformation, University of Hannover (see also PFG 6/2005, pages 465–524).

## 1 Introduction

Linear CCD array sensors have been widely used to acquire panchromatic and multispectral images in pushbroom mode for photogrammetric and remote sensing applications. IKONOS, successfully launched on 24 September 1999, was the first civilian satellite with high-resolution sensors, acquiring panchromatic and multispectral images with 1-m and 4-m ground pixel size respectively. IKONOS can acquire two (stereo) or more images of the same region quasi simultaneously by agile pointing of the sensor through rotation of the satellite body, reducing thus the differences between these images and facilitating automated mensuration processes. This fact, together with the high spatial resolution of the images, the 11-bit quantization and the narrow field-of-view allows and requires an extension of the "classical" satellite image processing methods for the full exploitation of the potential of this data.

In recent years, a large amount of research has been devoted to the efficient utilization of these high spatial resolution images, and in particular regarding sensor modelling and image orientation (BALTSAVIAS et al. 2001, JACOBSEN 2003, GRODECKI & DIAL 2003, FRASER et al. 2002, FRASER & YAMAKAWA 2003, EISENBEISS et al. 2004) and automatic DSM/DTM generation (TOUTIN 2004, ZHANG & GRUEN 2004, POON et al. 2005).

In this paper, we first briefly report about the key algorithms on automatic triangulation. Then, we present an advanced image matching method and give a detailed DSM accuracy evaluation using IKONOS *Geo-level* images in a testfield in Thun, Switzerland, with large height range and very variable terrain relief and land cover, and a laser DSM as reference data. The images were acquired at different times and pre-processed with different calibration parameters. Our matching method was developed for automatic DSM generation from linear array images and provides dense, precise, and reliable results. The approach uses a coarse-to-fine hierarchical solution with a combina-

tion of several image matching algorithms and automatic quality control. Finally, we reveal and quantify errors in the interior orientation of the sensor and present a general and practical method for in-flight calibration.

## 2 Sensor Modeling and Block Adjustment

The imaging geometry of IKONOS is characterized by nearly parallel projection in along-track direction and perspective projection in cross-track direction. A rigorous model can be used to reconstruct the physical imaging geometry and to model transformations between object and image coordinate systems. Alternatively, Rational Function Models (RFMs) have recently drawn considerable interest in the remote sensing community. In particular, IKONOS is only supplied with rational polynomial coefficients (RPCs) instead of rigorous sensor model parameters, while RPCs are provided or can be derived for other optical satellite sensors as well. A RFM is generally the ratio of two polynomials derived from the rigorous sensor model and ground control and/or sensor orientation information. These models do not describe the physical imaging process but use a general transformation to describe the relationship between image and ground coordinates. If the RPCs are computed without Ground Control Points (GCPs) (as is the case, with the RPCs provided by Space Imaging (SI) for Ikonos), the geopositioning accuracy of the RPCs needs to be improved and a bias needs to be removed with a certain number of GCPs and an additional 2D transformation. For single typical size images, two translations are sufficient with Ikonos, while Quickbird exhibits more non-linearities and requires a higher order transformation, e. g. affine (EISENBEISS et al. 2004). GRODECKI & DIAL (2003) proposed a method to block-adjust high-resolution satellite images described by RFMs and illustrated the method with IKONOS examples, suggesting the use of a linear scale factor in scanning direction when the image is long, e. g. over 50 km.

With the supplied RPCs, the mathematical model used is

$$\begin{aligned} x + \Delta x &= x + a_0 + a_1x + a_2y \\ &= RPC_x(\varphi, \lambda, h) \\ y + \Delta y &= y + b_0 + b_1x + b_2y \\ &= RPC_y(\varphi, \lambda, h) \end{aligned} \quad (1)$$

where,  $a_0$ ,  $a_1$ ,  $a_2$  and  $b_0$ ,  $b_1$ ,  $b_2$  are the affine parameters for each image, and  $(x, y)$  and  $(\varphi, \lambda, h)$  the image and object coordinates of the points.

The block adjustment model expressed in equation (1) is justified for any photogrammetric camera with a very narrow field-of-view. Using this model, we expect that parameter  $b_0$  is used to absorb all along-track errors causing offsets in the scanning direction, while parameter  $a_0$  absorbs across-track errors causing offsets in the line CCD direction. Parameters  $b_1$  and  $a_2$  absorb shear effects caused by gyro drift during the image scan, while parameters  $a_1$  and  $b_2$  are used to absorb parts of the radial ephemeris error, and interior orientation errors such as focal length and a part of lens distortion errors. In our approach, we first used the RPCs to transform from object to image space and then using these values and the known pixel coordinates of GCPs we estimated either two translations (model RPC1) or all 6 affine parameters (model RPC2).

For satellite sensors with a narrow field of view like IKONOS, even simpler sensor models can be used, such as the 3D affine model (3DAFF) and the relief-corrected 2D affine (2DAFF) transformation. They are discussed in detail in BALTSAVIAS et al. (2001) and FRASER et al. (2002). Their validity and performance is expected to deteriorate with increasing area size and rotation of the satellite during imaging (the so-called forward scanning mode) which introduces non-linearities, and for the 3D affine model with increasing height range and poor GCP distribution.

In order to apply the block adjustment, a certain number of GCPs and tie points have to be collected. In our approach, these points can be measured manually, semi-au-

tomatically or fully automatically. In particular, ellipse fitting and line intersection methods are suitable for GCP measurements over typical suburban, urban and rural areas (FRASER et al. 2002, EISENBEISS et al. 2004). In the experiments, these methods yielded suitable results for orientation of high-resolution satellite imagery. Another technique of choice can be least squares template matching (BALTSAVIAS et al. 2001).

### 3 The Matching Approach

We have developed an image matching approach for automatic DSM generation from linear array images, which has the ability to provide dense, precise, and reliable results. Actually, with minor modifications regarding the sensor model, the procedure can be used and has been used for frame images as well. The approach uses a coarse-to-fine hierarchical solution with a combination of several image matching algorithms and automatic quality control. The new characteristics provided by the linear array imaging systems, i. e. the multiple-view terrain coverage and the high quality image data, are also efficiently utilized in this approach.

The approach essentially consists of several mutually connected components: the image pre-processing, the multiple primitive multi-image (MPM) matching, the refined matching and the system performance evaluation. The overall data flow of this matching approach is shown schematically in Fig. 1. The linear array images and the given or previously estimated orientation elements as used as input. After pre-processing of the original images and production of the image pyramids, the matches of three feature types (feature points, grid points and edges) in the original resolution images are found progressively starting from the low-density features in the lowest resolution level of the image pyramid. A TIN of the DSM is reconstructed from the matched features at each pyramid level by using the constrained Delauney triangulation method. This TIN in turn is used in the subsequent pyramid level for derivation of approximations and adaptive computation of some

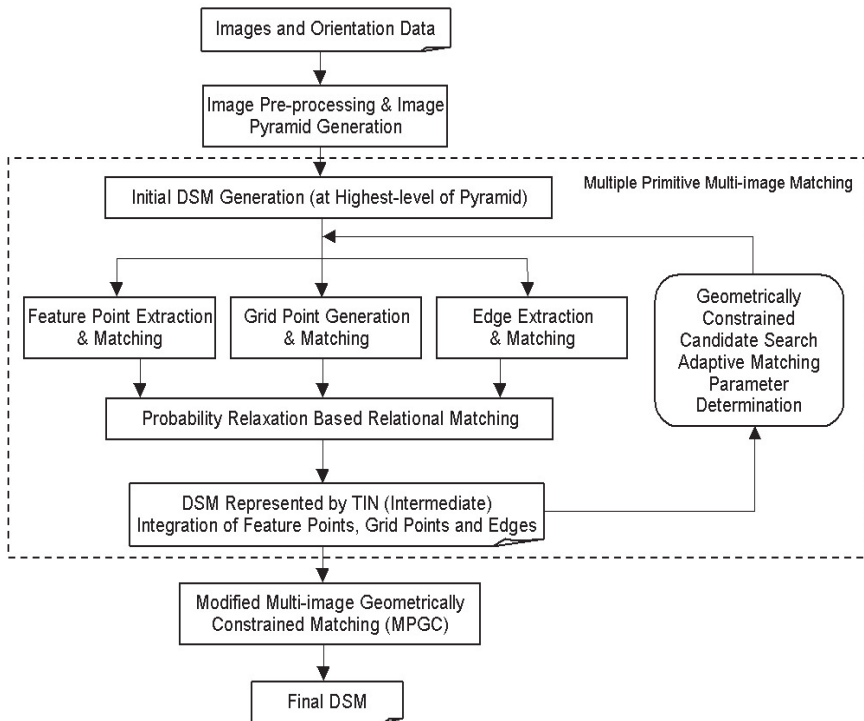


**Fig. 1:** Workflow of the automated DSM generation approach.

matching parameters. Finally, least squares matching is used to achieve more precise results for all matched features and for the identification of some false matches. At the end, a regular DSM grid is interpolated using a local neighbourhood and 2<sup>nd</sup> degree polynomial fit, without using breaklines explicitly. The procedure is characterized by the following:

1) **Multiple image matching:** We do not aim at pure image-to-image matching, but seek instead image-to-object correspondences. We have developed a new flexible and robust matching algorithm – the Geometrically Constrained Cross-Correlation (GCCC) method in order to take advantage of the multiple images. The algorithm is based on the concept of multi-image matching guided from object space and allows reconstruction of 3D objects by matching all available images simultaneously, without having to match all individual stereo-pairs and merge

the results. Only one image is used as template (reference), usually the nadir image if it is available. The cross-correlation coefficients of the template image with each of the remaining images are added, and then the maximum is found.

2) **Matching with multiple primitives:** We have developed more robust hybrid image matching algorithms by taking advantage of both area-based matching and feature-based matching techniques and utilizing both local and global image information. In particular, we combine the results of feature point and grid point matching through a probability relaxation based relational matching process, in order to enforce local consistency of the matching results, smooth spikes and select the best match points locally. The use of edges leads to preservation of surface discontinuities, while grid points bridge areas with little or no texture. With edge matching, even in areas of steep moun-

tains there are many successfully matched line features, which are necessary for modelling of very rough and steep terrain.

3) Self-tuning matching parameters: The adaptive determination of the matching parameters results in higher success rate and less mismatches. These parameters include the size of the correlation window, the search distance and the correlation threshold values. This is done by analyzing the matching results at the previous image pyramid level and using them at the current pyramid level.

4) High matching redundancy: With our matching approach, highly redundant matching results, including points and edges can be generated. Highly redundant matching results are suitable for representing very steep and rough terrain and allow the terrain microstructures and surface discontinuities to be well preserved. Moreover, this high redundancy also allows automatic blunder detection. Mismatches can be detected and deleted through analysis and consistency checking within a small neighbourhood of each match point.

5) Efficient surface modelling: The object surface is modelled by a triangular irregular network (TIN) generated by a constrained Delauney triangulation of the matched points and edges. A TIN is suitable for surface modelling because it integrates all the original matching results, including points and line features, without any interpolation. It is adapted to describe complex terrain types that contain many surface microstructures and discontinuities.

6) Coarse-to-fine hierarchical strategy: The algorithm works in a coarse-to-fine multi-resolution image pyramid structure, and obtains intermediate DSMs at multiple resolutions. Matches on low-resolution images serve as approximations to restrict the search space and to adaptively compute the matching parameters. The least squares matching methods are finally used to achieve sub-pixel accuracy for all matched features and identify some inaccurate and possibly false matches.

More details of this matching approach can be found in ZHANG & GRUEN (2004) and ZHANG (2005).

#### 4 Performance Evaluation

The study site is an area around the town of Thun, Switzerland. This area consists of a steep mountainous region in the south-western part and smooth hilly regions in the middle and northern parts. The town of Thun is located in the lower-middle part of the study area. The whole area is about  $17\text{ km} \times 20\text{ km}$  and 30% is covered by forests. The site has an elevation range of more than 1600 m (see shaded terrain model in Fig. 2) and the land cover is extremely variable.

Over this test area, three IKONOS image triplets (each covering ca.  $11\text{ km} \times 20\text{ km}$ ) were acquired, each triplet consisting of a stereopair and a nadir image. The first two image triplets (DEC\_O and DEC\_N) were acquired on the same day during winter time but were generated with different calibration parameters. These calibration parameters refer to the interior orientation of the sensor and allow an evaluation of the effect of interior orientation errors on DSM accuracy (see also section 5). In these two triplets, about 70% of the area was covered by snow, while sun elevation was very low (ca.  $19^\circ$ ) causing long shadows and low contrast. An-

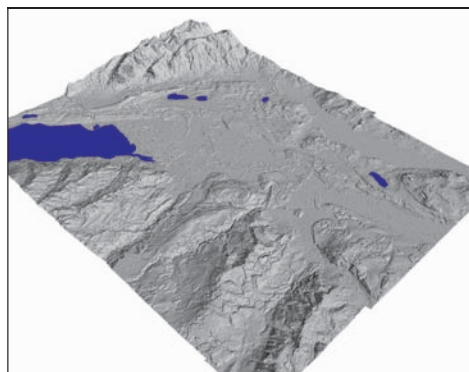


**Fig. 2:** Shaded terrain model (5 m grid spacing) of the whole study area (seen from the North) generated by image matching and the triplet – DEC\_N.

**Tab. 1:** Main characteristics of the three IKONOS image triplets acquired over the study area.

| Dataset | Acquisition & Generation Date | Sensor Azimuth | Sensor Elevation |
|---------|-------------------------------|----------------|------------------|
| DEC_O   | 2003-12-25<br>2004-01-19      | 180.39°        | 62.95°           |
|         | 2003-12-25<br>2004-01-19      | 72.21°         | 82.15°           |
|         | 2003-12-25<br>2004-01-19      | 128.17°        | 82.62°           |
| DEC_N   | 2003-12-25<br>2005-03-02      | 180.39°        | 62.95°           |
|         | 2003-12-25<br>2005-03-02      | 72.21°         | 82.13°           |
|         | 2003-12-25<br>2005-03-02      | 128.17°        | 82.62°           |
| OCT     | 2003-10-12<br>2004-02-11      | 10.74°         | 77.85°           |
|         | 2003-10-12<br>2004-02-11      | 4.69°          | 85.26°           |
|         | 2003-10-12<br>2004-02-11      | 197.09°        | 71.95°           |

other triplet (OCT) was acquired during autumn with no snow, less shadows and better illumination conditions (Tab. 1). All IKONOS images were Geo, 11-bit, with DRA (Dynamic Range Adjustment) off, and 1m panchromatic (PAN) and 4m multi-spectral (MS) channels (for DSM generation only the PAN images were used). For all IKONOS images, the RPCs were provided in the metadata files.

#### 4.1 Block adjustment

In order to precisely georeference the IKONOS images, about 50 well-distributed GCPs were collected with differential GPS in March 2004. The measurement accuracy was about 0.25 m. As expected, GCPs were difficult to find in rural and mountainous areas, but also in the town of Thun, where they had to be visible in all images simultaneously. Shadows and snow made their selection even more difficult. As a result, only

39 of them could be measured precisely in the images. The GCPs were measured in one of images of each triplet (usually the nadir) by the line intersection method and the conjugate points in the other images were computed with least squares matching.

Tab. 2 compares the results of the orientation of the first two IKONOS triplets (DEC\_O and DEC\_N) with different sensor models and different number of GCPs. All methods achieved RMSE values in East (X) and North (Y) direction of about half a meter. The maximum residuals were about 1 m in planimetry and 2 m in height. However,

**Tab. 2:** Comparison of sensor models and number of GCPs for the IKONOS triplet (DEC\_O) top and (DEC\_N) bottom regarding error statistics (in m). CPs are check points.

| Sensor Model | GCPs (CPs) | X-RMSE (max error) | Y-RMSE (max error) | Z-RMSE (max error) |
|--------------|------------|--------------------|--------------------|--------------------|
| RPC2         | 22 (0)     | 0.32 (0.70)        | 0.78 (1.53)        | 0.55 (0.78)        |
| RPC2         | 18 (4)     | 0.33 (0.80)        | 0.79 (1.48)        | 0.56 (1.41)        |
| RPC2         | 12 (10)    | 0.32 (0.73)        | 0.82 (1.64)        | 0.60 (1.04)        |
| RPC2         | 5 (17)     | 0.44 (1.04)        | 0.92 (1.83)        | 0.65 (1.15)        |
| RPC1         | 22 (0)     | 0.35 (0.82)        | 0.41 (0.91)        | 0.67 (0.80)        |
| 3DAFF        | 22 (0)     | 0.32 (0.73)        | 0.78 (1.50)        | 0.55 (0.78)        |
| RPC2         | 22 (0)     | 0.37 (0.70)        | 0.32 (0.79)        | 0.48 (1.07)        |
| RPC2         | 18 (4)     | 0.38 (0.79)        | 0.33 (0.75)        | 0.50 (0.98)        |
| RPC2         | 12 (10)    | 0.40 (0.92)        | 0.35 (0.85)        | 0.69 (1.66)        |
| RPC2         | 5 (17)     | 0.45 (1.08)        | 0.43 (0.96)        | 0.76 (1.86)        |
| RPC1         | 22 (0)     | 0.37 (0.76)        | 0.34 (0.66)        | 0.64 (1.26)        |
| 3DAFF        | 22 (0)     | 0.43 (0.89)        | 0.53 (0.90)        | 0.76 (1.83)        |

the results of the second triplet that was generated with new calibration parameters were better than those of the first triplet, especially in the North direction, due to interior orientation errors in the DEC\_O calibration (see also section 5). For the third triplet of OCT, it is not possible to make a comparison with the first two because in this triplet almost 50% of the area (northern part) was covered by clouds resulting in a different number and distribution of GCPs. However, even with the GCPs and check points (CPs) measured in the southern part of the images, the RMSE (RPC1) of the orientation was 0.30 m in East, 0.54 m in North and 0.77 m in height.

The results show that decreasing the number of GCPs down to 5 did not decrease the accuracy significantly, and that sub-meter accuracy can be achieved using only a few GCPs and the RPC models. The 3D affine (3DAFF) model also leads to accurate results, however with few GCPs the results

deteriorate significantly. For more detailed block adjustment results with different IKONOS datasets and different GCP distributions, see EISENBEISS et al. (2004). For the subsequent DSM generation, the sensor model RPC2 with all GCPs was used.

#### 4.2 DSM generation and evaluation

In order to quantitatively evaluate the accuracy of the generated DSM, a 2 m irregular-spacing laser DSM, with an accuracy of 0.5 m ( $1\sigma$ ) for bare ground areas and 1.5 m for vegetation areas, was used as reference data. The laser DSM was acquired in the year 2000 and provided by the Swiss Federal Office of Topography, Bern (Swisstopo). It only covers the southern part of the study area.

After all IKONOS image triplets were preprocessed by using the algorithms proposed in BALTSAVIAS et al. (2001) and the same parameters, our matching approach

**Tab. 3:** DSM accuracy evaluation results (in m) for three triplets, where, B1 – Bare ground; B2 – Bare ground (including mountainous area); B3 – Bare ground (including mountainous and shadow areas); C – City area only; V – Vegetation area only; W1 – Whole area; W2 – Whole area without vegetation areas. RMSE (95) and Average (95) are the RMS and average (with sign) height difference values after excluding the 5% largest differences.

|              |                        | triplet DEC_O |                      | triplet DEC_N |                      | triplet OCT   |                      |
|--------------|------------------------|---------------|----------------------|---------------|----------------------|---------------|----------------------|
| Terrain type | No. of compared points | RMSE Average  | RMSE(95) Average(95) | RMSE Average  | RMSE(95) Average(95) | RMSE Average  | RMSE(95) Average(95) |
| B1           | 7,037,578              | 1.27<br>0.82  | 0.93<br>0.89         | 1.15<br>0.31  | 0.73<br>0.37         | 1.41<br>0.22  | 0.95<br>0.21         |
| B2           | 7,993,875              | 1.84<br>0.92  | 1.04<br>0.92         | 1.90<br>0.34  | 0.93<br>0.35         | 1.77<br>0.29  | 1.09<br>0.29         |
| B3           | 9,763,257              | 2.11<br>0.80  | 1.20<br>0.80         | 2.14<br>0.29  | 1.19<br>0.30         | 1.75<br>0.29  | 1.07<br>0.29         |
| C            | 2,794,389              | 3.34<br>0.30  | 2.36<br>0.30         | 3.38<br>0.51  | 2.41<br>0.51         | 2.83<br>-0.25 | 2.08<br>-0.25        |
| V            | 8,689,642              | 8.16<br>1.68  | –                    | 8.05<br>1.58  | –                    | 6.61<br>-1.97 | –                    |
| W1           | 28,854,764             | 4.93<br>1.13  | 4.24<br>1.14         | 4.90<br>0.50  | 4.23<br>0.50         | 4.25<br>-0.40 | 2.96<br>-0.39        |
| W2           | 18,022,149             | 2.74<br>0.70  | 1.45<br>0.69         | 2.54<br>0.35  | 1.41<br>0.34         | 2.05<br>0.16  | 1.32<br>0.16         |

was applied. The three images of each triplet were matched simultaneously in order to achieve more reliable results. Some areas like lakes and rivers were manually defined as “dead areas” via a user-friendly interface and were excluded from matching. Taking the triplet DEC\_N as an example, the matching approach resulted in ca. 11 million points and 800,000 edges, of which more than 80% were labelled as highly reliable (quality indicator  $> 0.75$ ). This indicator varies from 0 to 1 and is computed through combination of various quality criteria like the cross-correlation coefficient, the slope of its maximum peak, the difference from the second highest peak etc.

Finally, three 5 m regular grid DSMs were interpolated from the raw matching results. Fig. 2 shows the shaded terrain model for the whole study area and Fig. 3 shows a comparison of the laser DSM and the results of matching for three sub-areas. As it can be seen, the resulting DSM reproduced quite well not only the general features of the terrain relief but also small geomorphological and other features visible in the IKONOS images. The resulting DSM showed many topographic details and different features, like small valleys in the mountains, detailed patterns related to streets and buildings in suburban and urban areas, linear features

related to highways and main road networks, sparse trees, small clusters of houses and forest areas.

A quantitative evaluation of the DSM was conducted by comparison with the laser DSM and nearly 28 million elevation points were used in statistical computations for the whole study area. We show here the results of the raw computations, without any a posteriori manual editing procedure applied. Tab. 3 gives the DSM accuracy evaluation results. We computed the differences as reference DSM minus the interpolated heights from our generated DSM. Differences more than 50 m (which were very few, in the worst case 0.03% of the total number of points, mostly in shadow areas and were not eliminated by the automatic blunder detection) were excluded. The accuracy of the generated DSM, excluding vegetation areas, is between 1.0–5 m, depending on the terrain relief and land cover. The results can be summarized as follows:

- High accuracy at meter or even sub-meter level can be achieved in bare ground areas. We could not select truly bare ground areas, instead our areas still contain many sparse trees and small clusters of houses. The analysis shows that in bare ground areas more than 70 percent of the points

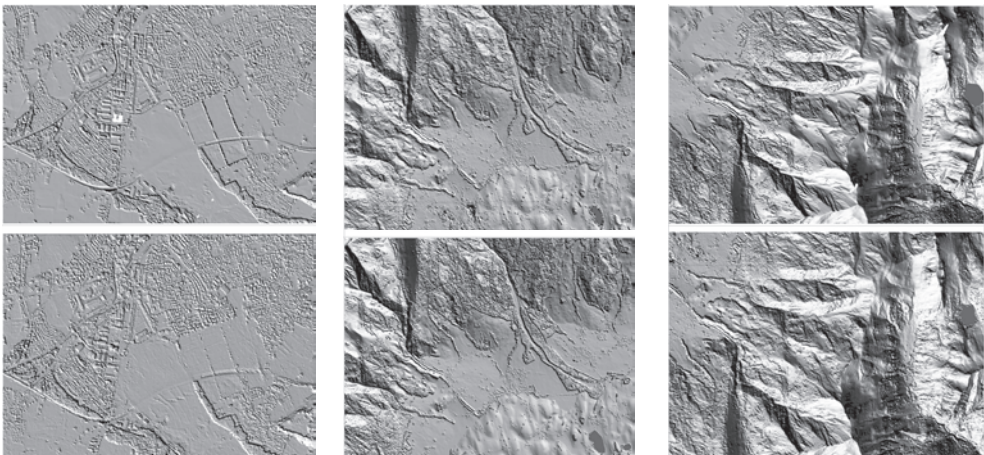


**Fig. 3:** Shaded terrain models of three sub-areas, where the right two show the mountain area, the middle two vegetation areas and the left two the area around the town of Thun. In each subimage: top, Laser DSM (2 m average point distance); bottom, results of matching from the T\_OCT triplet.



have differences of less than 1m. Around the areas of sparse trees and small houses, the resulting DSM is lower than the laser DSM. This can be expected because usually these small features were either smoothed out by our matching method or removed in the automated blunder detection procedure.

- A bias of about 1.0–1.5 m can be observed in the DEC\_O results caused mainly by interior orientation errors. A part of the bias is also due to the 3 years difference between acquisition of the laser DSM and the Ikonos images, and regarding the vegetation due to the different state of the trees (in the October triplet and the laser data with leaves, in the December ones without). The difference of the average for case V between the OCT and the DEC triplets is exactly due to the different state of the trees. The same reason causes the difference of the average for cases C and W1 between the same triplets. Another factor that introduces systematic differences is the snow existing in the December images. While in the flat areas the snow thickness could be in the order of few cm to dm, in the higher regions it could reach 1 m or more.
- In urban and forest areas the accuracy becomes worse, which is due to the fact that the reference laser measurements and the DSM determined in matching may refer to partly different objects. Usually, the generated DSM should be higher than the laser DSM in forest areas (laser can sometimes penetrate the tree canopy) and narrow low-lying objects (like streets in very dense residential areas). This is not the case for the DEC triplets and especially the vegetation due to the different state of the trees and partly the smoothing performed in matching during blunder elimination. However, for large buildings, the two DSMs coincided quite well.
- Other factors that influenced the matching were the long and strong shadows and occlusions, especially in the mountain areas, and very low textured snow areas. However, after our particular preprocessing the long and strong shadows combined

with the influence of the lower sun elevation are good for DSM generation in bare ground areas because they seem to generate more image texture information (finer radiometric differences are better visible) with less noise.

- In steep mountain areas (slope more than  $70^\circ$ ), there are also some blunders with more than 400 m height difference. They are mainly caused by occlusions. In addition, the smoothness constraints smoothed out some steep and small features of the mountain areas (mainly in shadow areas) because there were not enough extracted and matched edges.
- In addition, the difference values show some stripe-like patterns for triplet DEC\_O (Fig. 6) and OCT. In these stripes, the height difference values show a jump of about 1.3-1.5 m. These patterns, however, do not appear in the dataset of DEC\_N (Fig. 6). The reason for these stripes is explained in section 5.
- The RMSE values of the OCT triplet compared to the ones of the DEC\_O (with the same interior orientation) show a slight improvement due to better illumination conditions and less shadows. This is evident especially in cases B3 and C. However, the difference is not very big, which stresses the importance of an appropriate preprocessing of the images in order to improve image quality for matching.

Taking all above factors into account, it becomes clear that IKONOS has a very high geometric accuracy potential and with sophisticated matching algorithms a height accuracy of around 1 m can be achieved in bare ground areas.

## 5 In-Flight Calibration and Determination of Interior Orientation Parameters

In-flight calibration is important for satellite sensors, since during launch the environmental conditions change rapidly and drastically and this usually causes changes in the internal sensor geometry, which is determined in a pre-launch calibration. Further-

more, when the camera is large some of the interior orientation parameters cannot be determined with a laboratory calibration (Space Imaging, personal communication). The environmental conditions after orbit stabilisation are also harsh and may cause internal geometry changes, however this is not as crucial as the changes that occur during launch. For these reasons, an inflight-calibration is usually a must and companies operating satellites take measures to perform such calibration, sometimes with the use of testfields and many accurate, often signalised GCPs. The establishment and maintenance of such testfields is difficult and costly. Inflight-calibration may not permit the determination of all internal geometry sensor parameters. This is even more the case with high-resolution satellites, like Ikonos, with a very narrow field-of-view and many internal geometry parameters and a complicated focal plane arrangement of multiple CCD linear arrays. In this case, many of the sensor parameters are highly correlated and not determinable. One may argue, that with the help of GCPs and use of RPCs, errors in the interior orientation parameters are absorbed without any negative effect in the determination of planimetric and 3D coordinates of ground points. However, as we will show below, some possible interior orientation errors, cannot be modelled by RPCs and can decrease the accuracy of 3D point positioning significantly. This is a problem for applications requiring very high accuracy, exploiting the full accuracy potential of satellites like Ikonos and Quickbird which lies in the 3–4 dm and 5–6 dm level for planimetry and height respectively (FRASER et al. 2002).

The design of the Ikonos focal plane is quite complicated. It consists of two TDI panchromatic CCD arrays, one for reverse and one for forward mode scanning, the TDI having 32 stages. In the reverse scanning the earth surface is imaged from North to South (independently of the sensor azimuth), in the forward from South to North, which means a continuous and quasi constant rotation of the satellite body. The number of TDI stages used is programmable

from the ground and is often 13. Furthermore, there are 4 multispectral arrays, without TDI. The two panchromatic and the multispectral arrays consists actually of 3 separate CCDs that are mechanically butted to form a long line. The Ikonos focal plane is shown in Fig. 4. The reason for use of 3 CCDs is probably that at the time of the sensor production a single CCD with that length was not possible. An additional reason can be that Kodak preferred for production speed, cost and reliability reasons to use standard, off-the-shelf and tried components. This sensor design is mentioned, although sometimes vaguely, in few SI papers, but it is not widely known. The length of each of the 3 CCDs is unknown, but we estimate it, based on a published photograph, to be about 5,000 pixels, allowing an overlap between the 3 CCDs of sufficient width. The central of the 3 CCDs is offset from the other two in the direction vertical to the CCD lines, while in the CCD line direction, the central CCD overlaps with the other two. This overlap allows radiometric and geometric corrections when stitching the 3 CCD line images to one. SI could perform geometric corrections, e. g. by matching of corresponding points in the overlap regions and adjusting the geometry of the partial images, but clearly matching could lead to some errors, especially in textureless areas, although this could be easily circumvented by using

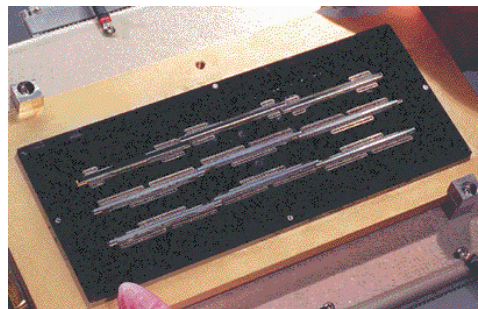


**Fig. 4:** The Ikonos focal plane showing the 3 CCDs forming each CCD row. We believe that the 3 CCD rows from top to bottom show the multispectral CCDs (each with 4 spectral channels), and the reverse and forward panchromatic CCDs with TDI (each with 32 stages (lines) (Copyright Space Imaging).

many images and many match points, to compute some simple corrections of the interior orientation which are stable for a period of few days or even months. Radiometric corrections are apparently performed. If the geometry of these 3 CCD lines is known and stable, then stitching the 3 images together should not be a problem. However, due to changes in the internal sensor geometry during and after launch, as mentioned above, the relative geometry of the 3 CCDs forming one virtual long line will not remain stable. Various deformations (shifts, rotations, etc.) may occur in the focal plane and out-of-plane, the most probable ones being shifts and rotations in the focal plane. Such problems may occur not just with Ikonos, but any sensor forming a virtual line from multiple single CCD lines, and independently of the way the CCDs are butted (optically, mechanically, through use of multiple lenses etc.). For Quickbird, possible errors are even more, since this sensor has a similar focal plane geometry as Ikonos, but with 6 CCDs (instead of 3) forming the virtual CCD line. The 6 partial CCD images are obvious in many Quicklooks in the Digital Globe archive, due to radiometric differences between them. Again the fact that Quickbird uses 6 CCDs to form a line is not widely known. For both Quickbird and Ikonos, the RPCs are computed for a whole image formed by the virtual CCD line, and thus deformations of the single CCDs can not be modeled.

First DSM accuracy analysis and visualisation of errors using the Thun testfield showed the stripes of Fig. 6 (left). The average height jump at profiles P3 and P4 was 1.5 m and at P1 and P2 1.3 m, corresponding to a parallax error in  $y$  (scanning direction) of about 0.7–0.8 pixels, while the  $x$ -parallax error was only 0.15–0.2 pixels. A first thought was that these stripes could be due to laser scanner errors. Neighbouring laser scanner strips may exhibit offsets, tilts etc., if the strips are not tied together appropriately in a common adjustment. This was even more probable as the Thun region was the very first region in Switzerland that was covered with laser scanner data and at that

initial stage the Swisstopo but also the companies performing the data collection, processing and editing had relatively little experience. The Thun region, among all Swiss territory covered with laser scanner data, is estimated by the Swisstopo to be the region with the least accurate laser DSM. However, the distance between the stripes observed in Fig. 6 (left) was too large compared to the laser scanner swath, and the fact that they were two, and approximately at the overlap regions of the 3 CCDs was quite suspicious. To verify the assumption of interior orientation errors of the Ikonos sensor, the following procedure was followed. First, the Ikonos quicklooks were used to find the approximate position of the overlap regions (and possible seam lines between the 3 CCDs). The quicklooks are the raw data, after stitching, with a spatial resolution of about 16 m. Then, these regions were transferred to the Geo images using corresponding points. Next, we identified areas that were almost totally flat in these overlap regions. We then matched semi-automatically with least squares matching in the Geo forward and backward images of the stereopair of the triplet DEC\_O very dense points along a profile that was vertical to each of the two overlapping regions (stripes). In these flat regions, interior orientation errors were visible as parallax jumps along the profiles. The above calibration procedure is not optimal as a) it requires flat regions and b) matching errors along one single profile, due e. g. to lack of texture, may cause parallax jumps. A more appropriate in-flight calibration procedure will be outlined below.

The fact that errors appear only in vertical stripes is easily understandable. A shift, e. g. in the middle of the 3 CCDs, will be stable during the quasi-simultaneous image acquisition of a stereopair or triplet, and thus for object points imaged at the same CCD no  $y$ -parallax (in the scanning direction) will be introduced (the planimetric position of such points will be shifted, but their height will be similar apart from positions of abrupt height discontinuities). However, ground points imaged at different CCDs will exhibit parallax (and height) errors. This will al-

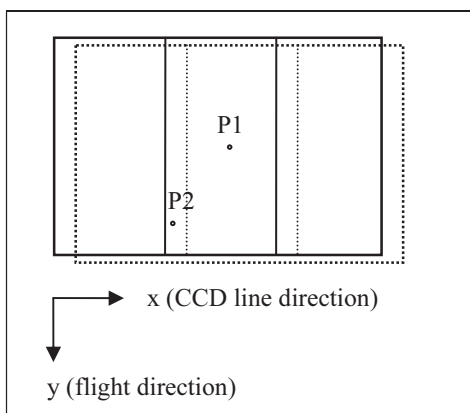


**Fig. 5:** The cause of vertical stripes with larger height error due to inaccurate interior orientation modelling. E. g. a possible shift of the middle CCD relative to the other two will cause the same pixel coordinate error for point P1, but not for point P2, introducing thus a y-parallax (and height) error.

ways happen as the pointing accuracy of Ikonos on the ground is in the order of few hundred meters. The width of the vertical stripes will vary depending on the pointing accuracy of the sensor but also on scale differences in the area between the different Ikonos images. An example is shown in Fig. 5 with the images of a stereopair (e. g. forward and backward) separated in 3 parts, each representing the part imaged by each of the 3 linear CCDs. Point P1 is imaged in both images in the middle CCD, and thus a possible relative shift of this CCD with respect to the other two will be the same in both images. However, point P2 is imaged in the middle and left CCDs and thus a relative shift between them will lead to a y-parallax and respective height error.

A better in-flight calibration procedure uses the very dense matching results and their differences from the reference data (e. g. laser DSM) in open, not rugged areas, ideally with enough texture to allow accurate matching. Thus, areas with trees, bushes, urban areas etc. were excluded, and areas shown at the position of profiles P1 to P4 (see Fig. 6, left) were selected. These profiles can actually be rectangular areas along the stripes to allow a high number of height differences to be used in the further

analysis. The high number allows a smoothing of matching errors and errors of the reference data and also an elimination of large differences due to few single trees and buildings included in the rectangle. As already mentioned, the accuracy of our matching algorithm in open terrain is 1 m or less. Through averaging of many height differences, we anticipate to estimate the height jump with an accuracy 0.3–0.5 m, depending also on the quality of the reference data. At the position of each profile the height jump at the left and right side of each profile is computed through averaging of values to the left and right side of each jump. The estimation of the jump at the left and right side of each profile allows to estimate whether there is only a shift between the 3 CCDs or also a rotation. The above procedure can be used as a general in-flight calibration method to determine such interior orientation errors. The reference data may come from any source and should have an accuracy of a few dm. In this respect, the laser data used here were not optimal, as their accuracy (one sigma) at open terrain was 0.5 m and they had some artifacts (see below and Fig. 6). The terrain does not have to be flat (undulating terrain is fully sufficient), while no signalised points are needed.

The above analysis with the DEC\_O was made in April 2004 but was not published for various reasons. After personal contacts with SI and verification of the encountered problems, SI performed a new more accurate determination of the Ikonos internal geometry, and the December 25<sup>th</sup> images were processed with this new calibration (DEC\_N), while the October images were still with the old calibration. It is unknown how this new calibration was performed by SI, but possibly using testfield(s). A comparison of Fig. 6 left and right shows a significant improvement with the new calibration and no apparent stripes and height jump in Fig. 6 right. It also stresses the importance of performing a frequent in-flight calibration by the companies operating satellites. The influence of the new calibration on the 3D po-

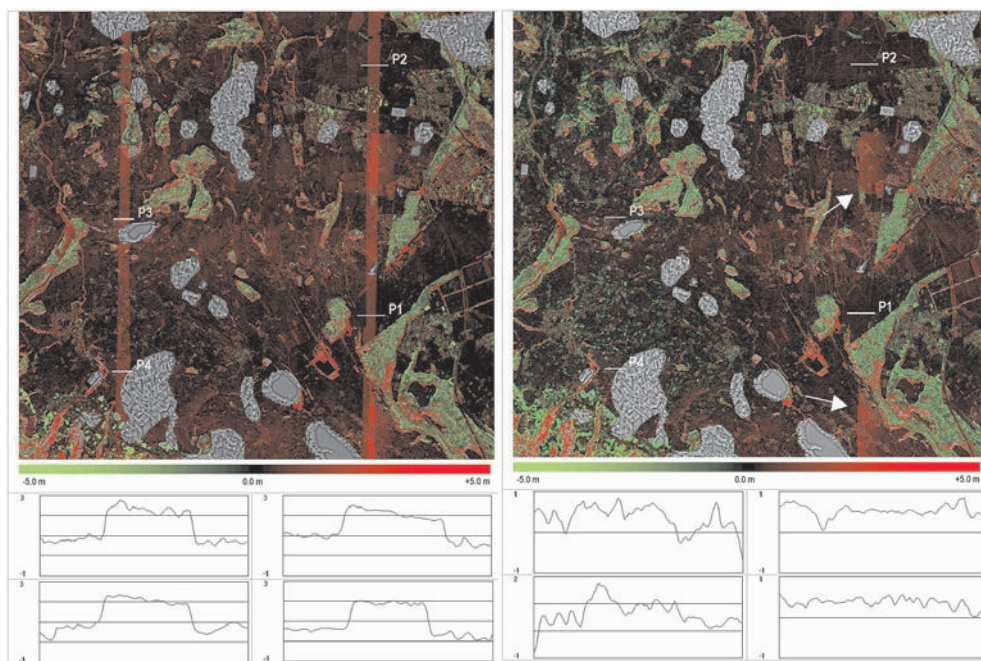


**Fig. 6:** Accuracy analysis based on colour coded height differences (in green and red negative and positive values, respectively). The height differences were computed from the reference DSM and the interpolated heights from the DSM generated by matching. At the bottom, the height differences along 4 profiles (P1 to P4, in the same sequence as shown in the top images). Left: for image triplet DEC\_O. Right: for image triplet DEC\_N after the new improved interior orientation determination.

sitioning accuracy is also shown in the Y-RMSE values of Tab. 2 and the average error values of cases B1, B2 and B3 of DEC\_O and DEC\_N in Tab. 3. An analysis of the October images showed a jump at both overlap regions, however, the width of the jump was smaller. The width of the overlap depends mainly on the across-track pointing accuracy of the satellite. It is also influenced by scale differences between the images, the stripes becoming more apparent when the scale differences increase (which is the case when the stereopair images are not symmetric with respect to the nadir or the terrain slope in flight direction is large).

The differences between laser DSM and the matching results of all triplets showed some systematic artifacts, see arrows in Fig. 6 right. These are attributed to errors in the laser DSM. It is scientifically very interesting to see that sophisticated matching methods and satellite images from 680 km

flying height can reveal errors in airborne laser scanning, although this is certainly not a cost-effective method for quality control of DSMs generated by laser scanning.

## 6 Conclusions

We presented processing of Ikonos triplet images over a testfield in Thun, Switzerland with accurate ground control points, 1600 m height range, variable land cover and sub-optimal imaging conditions (snow, long shadows). A sophisticated matching algorithm for DSM generation was presented and the results were compared to reference data from airborne laser scanning. The RMS errors for the whole area, excluding vegetation, were 2–3 m, while for bare ground the accuracy is about 1 m or less. As evidenced by the visual inspection of the results, our matching method can reproduce not only the general features of the terrain

relief, but also detailed features of relief. The results were partly influenced by the suboptimal accuracy of the reference DSM and its temporal difference from the acquisition of the Ikonos images. The largest errors usually occurred in the shadow, tree and building covered areas and the best results were obtained in bare ground areas. If the bias introduced by trees and buildings is taken out, we can expect a height accuracy of one pixel or even better from IKONOS imagery as "best case" scenario. A major problem of our automatic DSM generation approach is the automated detection of small blunders, which still exist in the results. This constitutes a relevant topic for further research.

The accurate matching allowed the detection and quantification of errors in the interior orientation of the sensor, caused by changes in the relative position of the 3 CCDs forming the virtual CCD line. These errors were verified through a cooperation with Space Imaging and recomputation of the sensor interior orientation. The interior orientation errors caused height jumps of 1.3 to 1.5 m along two stripes at the overlap regions of the 3 CCDs. The method used for the detection and quantification of these errors is applicable for in-flight calibration of sensors forming a virtual image through butting of multiple CCD arrays, without the need of testfields with signalised points, which are difficult to establish and maintain. Depending on the accuracy of the matching method and of the reference DSM, we estimate that this in-flight calibration method can detect interior orientation errors causing parallax errors of 0.3–0.5 pixels or more.

### Acknowledgements

We acknowledge the support of Space Imaging USA by provision of the images and fruitful discussions and the support of the Swiss Federal Office of Topography, Bern, which provided the laser DSM.

### References

- BALTSAVIAS, E.P., PATERAKI, M. & ZHANG, L., 2001: Radiometric and Geometric Evaluation of IKONOS Geo Images and Their Use for 3D Building Modeling. – Joint ISPRS Workshop on „High Resolution Mapping from Space 2001“, Hannover, Germany, 19–21 September.
- EISENBEISS, H., BALTSAVIAS, E.P., PATERAKI, M. & ZHANG, L., 2004: Potential of IKONOS and QUICKBIRD Imagery for Accurate 3D-Point Positioning, Orthoimage and DSM Generation. – IAPRS, Vol. **35** (B3): 522–528.
- FRASER, C., BALTSAVIAS, E.P. & GRUEN, A., 2002: Processing of IKONOS Imagery for Sub-meter 3D Positioning and Building Extraction. – ISPRS Journal of P&RS, **56** (3): 177–194.
- FRASER, C. & YAMAKAWA, T., 2003: Applicability of the Affine Model for IKONOS Image Orientation Over Mountainous Terrain. – Joint ISPRS/EARSeL Workshop on High-Resolution Mapping from Space 2003, Hannover, Germany, 6–8 October (on CD-ROM).
- GRODECKI, J. & DIAL, G., 2003: Block Adjustment of High-Resolution Satellite Images Described by Rational Polynomials. – PE&RS, **69** (1): 59–68.
- JACOBSEN, K., 2003: Geometric Potential of IKONOS- and QuickBird-Images. – In: FRITSCH, D. (Ed.): Photogr. Week '03, pp. 101.
- POON, J., FRASER, C., ZHANG, C., ZHANG, L. & GRUEN, A., 2005: Quality Assessment of Digital Surface Models Generated from IKONOS Imagery. – Photogrammetric Record, **20** (110): 162–171.
- TAO, C.V. & HU, Y., 2001: A Comprehensive Study of the Rational Function Model for Photogrammetric Processing. – PE&RS **66** (12): 1477–1485.
- TOUTIN, TH., 2004: Comparison of Stereo-Extracted DTM from Different High-Resolution Sensors: SPOT-5, EROS-A, IKONOS-II, and QuickBird. – IEEE Transactions on Geoscience and Remote Sensing, **42** (10): 2121–2129.
- ZHANG, L., 2005: Automatic Digital Surface Model (DSM) Generation from Linear Array Images. – Ph. D. Diss., Inst. Geodesy and Photogrammetry, ETH Zurich, No. 88.
- ZHANG, L. & GRUEN, A., 2004: Automatic DSM Generation from Linear Array Imagery Data. – IAPRS, Vol. **35** (B3): 128–133.

Address of the authors:

Dr. Sc. techn. EMMANUEL BALTSAVIAS  
 Dr. Sc. techn. LI ZHANG  
 Dipl.-Ing. HENRI EISENBEISS  
 Institute of Geodesy and Photogrammetry  
 ETH-Hoenggerberg, CH-8093 Zurich,  
 Tel.: +41-1-633 (3042, 3604, 3287)  
 (manos,zhang,ehenri)@geod.baug.ethz.ch

Manuskript eingereicht: Juni 2005

Angenommen: Juli 2005